Letter

Second dome of superconductivity in $YBa_2Cu_3O_7$ at high pressure

Johannes Nokelainen,[1,2,3,4,*] Matthew E. Matzelle,[1,2] Christopher Lane,[5] Nabil Atlam,[1,2] Ruiqi Zhang,[6] Robert S. Markiewicz,[1,2] Bernardo Barbiellini,[4,1,2] Jianwei Sun,[6] and Arun Bansil[1,2,†]

[1]*Department of Physics, Northeastern University, Boston, Massachusetts 02115, USA*
[2]*Quantum Materials and Sensing Institute, Northeastern University, Burlington, Massachusetts 01803, USA*
[3]*Department of Physics and Astrophysics, Howard University, Washington, DC 20059, USA*
[4]*Department of Physics, School of Engineering Science, LUT University, FI-53850 Lappeenranta, Finland*
[5]*Theoretical Division, Los Alamos National Laboratory, Los Alamos, New Mexico 87545, USA*
[6]*Department of Physics and Engineering Physics, Tulane University, New Orleans, Louisiana 70118, USA*

(Received 9 May 2023; revised 16 April 2024; accepted 4 June 2024; published 11 July 2024)

Evidence is growing that a second dome of high-T_c superconductivity can be accessed in the cuprates by increasing the doping beyond the first dome. Here, we use *ab initio* methods without invoking any free parameters, such as the Hubbard U, to reveal that pressure could turn $YBa_2Cu_3O_7$ into an ideal candidate for second dome superconductivity, displaying the predicted signature of strongly hybridized $d_{x^2-y^2}$ and d_{z^2} orbitals. Notably, pressure is found to induce a phase transition replacing the antiferromagnetic phases with an orbitally degenerate $d-d$ phase. Our study suggests that the origin of the second dome is correlated with the oxygen-hole fraction in the CuO_2 planes and the collapse of the pseudogap phase.

DOI: 10.1103/PhysRevB.110.L020502

In the search for superconductivity (SC) at higher temperatures, one of the more intriguing possibilities is that the high-T_c cuprate superconductors also feature another superconducting dome in the extremely overdoped metallic and nonmagnetic (NM) regime [1–14]. This is in stark contrast to the long-studied "first dome" that can be characterized as a lightly doped Mott insulator with a partially occupied Cu $d_{x^2-y^2}$ band and short-range antiferromagnetic (AFM) order [15]. Evidence for the existence of such a "second dome" has been building in recent years, as SC has been observed even when the doping levels have been driven far beyond the first dome via high-pressure oxygenation (HPO) synthesis [13]. Findings of $T_c = 95$ K in Sr_2CuO_{4-y} [1] and $T_c = 70$ K in Ba_2CuO_{4-y} [7] have heightened interest since these T_c's are clearly higher than $T_c \sim 44$ K of their isostructural counterpart $La_2CuO_{4+\delta}$. Also, a variety of other types of unconventional superconductors have been shown to feature two or more SC domes with distinct characteristics [16–21].

To explain the second dome, Maier *et al.* have constructed a model where the valency is increased by introducing holes on the Cu d_{z^2} orbitals, resulting in a new peak in the pairing function [8,9]. Similar models [5,14] have been invoked to explain the presence of a second dome in a single CuO_2 plane grown on top of $Bi_2Sr_2Ca_{n-1}Cu_nO_{2n+4+\delta}$ (BSCCO), $n = 2$ [4]. However, this system is not practical for transport measurements, while for the HPO cuprates the polycrystalline samples contain many SC phases with a multiplicity of oxygen vacancy orderings and it is unclear which of the phases are the best superconductors [11].

Besides chemical doping, pressure (P) is also known to increase doping levels [22] and enhance T_c in a number of cuprates [23]. Pressure has also been observed to trigger a second, anomalous, rise of T_c in BSCCO, $n = 1, 2, 3$; when the pressure is applied to optimally doped samples, T_c first decreases but then increases into a second dome [3,10]. However, the notoriously complicated multiphase structure of BSCCO involving supermodulation and complex oxygen ordering [24–26] makes it difficult to characterize the underlying physics and the second dome has not been observed in other recent studies [27,28].

Here, we present an *ab initio* study of pressure-induced doping of the prototypical cuprate superconductor $YBa_2Cu_3O_7$ ($YBCO_7$) and discuss its high-pressure states from the viewpoint of the second dome physics. $YBCO_7$ offers the advantages that it is in the overdoped regime yet stoichiometric, as illustrated in Fig. 1(a). Thus, pressure can more easily drive the material to the extremely overdoped regime in which the structure remains single phase, reducing the challenges associated with complex distributions and pressure effects of dopant atoms. Our first-principles computations employ the strongly constrained and appropriately normed (SCAN) density functional [29–32], which has been shown to provide a good parameter-free first-principles description of electronic correlation and Cu–O charge transfer physics [33–41]. Various magnetic orders are considered under hydrostatic pressure, which we increase adiabatically from zero up to 170 GPa. The Supplemental Material (SM) [42] contains the details of our computations. Our analysis shows that pressure induces three key effects in $YBCO_7$ that facilitate the transition to the second dome:

(1) Change in the pyramidal Cu–O environment. Figure 1(d) presents the pressure evolution of several structural parameters. There are no substantial structural differences

*Contact author: j.nokelainen@northeastern.edu
†Contact author: ar.bansil@northeastern.edu

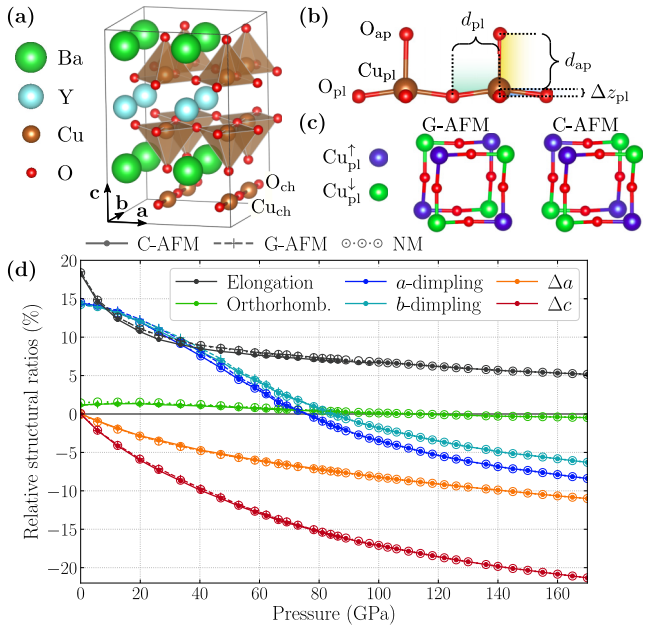

FIG. 1. (a) Atomic structure of $YBCO_7$. Cu_{pl} atoms reside in pyramidal cages formed by the O_{pl} and O_{ap} atoms. The CuO_2 planes are separated by a Y buffer layer. Sandwiched between the BaO layers are the CuO chains, which contain the oxygen dopants. Note that $YBCO_7$ is the fully doped compound of the $YBCO_{6+\delta}$ family with complete CuO chains, while $YBCO_6$ is the undoped system in which all the O_{ch} sites are vacant. The chains are arranged along the b axis, which is 1.2% longer than the a axis ($a_0 = 3.83$ Å). (b) Definitions of the d_{pl} and d_{ap} Cu–O distances and Δz_{pl}. (c) Schematics of the G-AFM (C-AFM) magnetic configuration that has antiferromagnetic (ferromagnetic) interlayer coupling of the Cu_{pl} ions across the Y buffer layer. (d) In % units, P evolution of relative elongation of the Cu–O pyramids $(d_{ap} - d_{pl})/d_{pl}$, relative orthorhombicity of the unit cell $(b - a)/a$, dimpling ratio $\Delta z_{pl}/d_{pl}$ (separately for the a and b directions), and lattice parameter modifications $\Delta a = (a - a_0)/a$ and $\Delta c = (c - c_0)/c$.

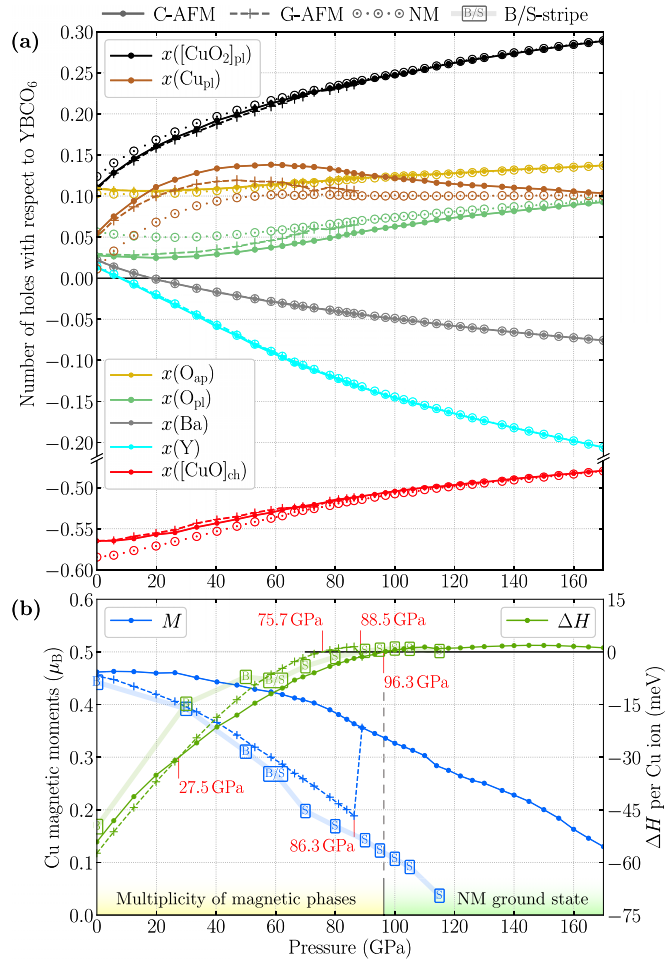

FIG. 2. (a) Hole contents for various ions and groups obtained as Bader charge differences between $YBCO_7$ and the undoped base compound $YBCO_6$ (see SM Sec. S3 [42] for details). (b) Left axis: Pressure evolution of the Cu_{pl} magnetic moments. Right axis: Magnetic enthalpy $\Delta H = H_{AFM} - H_{NM}$.

between the NM state and the G-AFM and C-AFM orders [see Fig. 1(c) for definitions]. The lattice constants are in excellent agreement with Ref. [43] (within 0.4% at $P = 0$ and 0.7% at $P \approx 12.7$ GPa). However, we did not observe the structural instabilities found in Ref. [44] (see SM Sec. S6 [42] for details). As is typical of layered materials such as the cuprates, the c axis shrinks more rapidly than the a and b axes (e.g., at 140 GPa c has decreased by about 20% while a and b have decreased by about 10%). Concurrently, there is a decrease in the elongation of the pyramidal Cu–O cages, which is intimately connected to the relative energies of the Cu $d_{x^2-y^2}$ and d_{z^2} orbitals. Interestingly, enhanced elongation is known to be favorable for the first dome of SC [45] while the opposite seems to be the case in Ba_2CuO_{4-y} [7]. $YBCO_7$ has a relatively large elongation of about 18% but it is quickly reduced under pressure and at 170 GPa it is only about 5%. Notably, the strong dimpling [Fig. 1(b)] of 14.2% is reduced under pressure until it reverses sign at 80 GPa such that the Cu_{pl} atoms bulge out from the pyramids towards the Y layer. At 170 GPa the dimpling is −8.4% (−6.3%) in the a (b) direction. Also the slight nonorthorhombicity ($b > a$) of 2% is removed under pressure and weakly reversed above 120 GPa.

(2) Pressure-induced doping. Figure 2(a) presents the hole contents (x) based on the Bader charge analysis [46,47]. The zero-pressure doping on the CuO_2 planes is $x([CuO_2]_{pl}) = x(Cu_{pl}) + 2x(O_{pl}) = 0.11$ holes [48] and the CuO chains assume a negative doping of $x([CuO]_{ch}) = -0.57$ holes, with weak magnetic configuration dependence. This reflects charge transfer from the CuO_2 planes to the CuO chains as $YBCO_6$ is doped to $YBCO_7$. Significant doping (0.11 holes) is found also on the O_{ap} sites. Under pressure, the CuO_2 plane is doped further up to 0.28 holes at 170 GPa, an increase of 0.17 holes over the zero-pressure value. The sources of this doping are the Ba and Y ions, which capture electrons at an almost linear rate until about 60 GPa, after which this electron capture rate slows down, especially for Ba. This could simply be the result of the large ionic radii of Y and Ba. When the lattice contracts under pressure, e–e repulsion would tend to force the electrons to migrate from the tightly packed CuO_2 planes to the buffer layers with a smaller electron density. Interestingly, the P-induced doping has been previously attributed only to the CuO chains, either due to an increased charge transfer between the chains and the CuO_2 planes or to the

reordering of the O_{ch} vacancies [49–52]. However, we find that the chains also become doped with 0.09 holes over the pressure range considered.

The distribution of the doping within the CuO_2 planes deserves special attention. Below $P \approx 40$ GPa, $x(Cu_{pl})$ grows rapidly while $x(O_{pl})$ stagnates, i.e., the additional doping ends up on the Cu ions. But this trend starts to change at higher pressures. Beyond 80 GPa the situation is reversed; $x(Cu_{pl})$ even starts to decrease while $x(O_{pl})$ grows steadily. We will return to discuss the implications of this behavior below.

(3) Stabilization of the NM state. Figure 2(b) presents the Cu_{pl} magnetic moments (M) and enthalpies relative to the NM phase (ΔH) for the studied magnetic phases. At zero pressure the G-AFM and C-AFM states and a 3×2 bond-centered stripe phase (B stripe) [53] are below the NM state by 57, 54, and 50 meV, respectively, which is consistent with the multiplicity of near-degenerate magnetic phases found in Ref. [36]. A direct effect of the pressure-induced doping is the suppression of the magnetic moments. $M_{\text{G-AFM}}$ and M_{stripe} start to decrease as soon as pressure is applied, but $M_{\text{C-AFM}}$ is robust up to 30 GPa before it starts to decrease. The pressure also decreases the stability of the magnetic phases, but the competition between them persists. The C-AFM state becomes the new ground state over the G-AFM state at 27.5 GPa. The G-AFM state further rises above the NM phase at 75.7 GPa and transitions to the C-AFM state at pressures beyond 86.3 GPa. The B stripe also goes through a phase transition into a site-centered stripe phase (S stripe) around 60 GPa (where it shows mixed characteristics) and rises above the NM phase at 88.5 GPa. Finally, the C-AFM state becomes metastable at 96.3 GPa so that the NM state is the ground state at high pressures. In this NM region, we were able to preserve the C-AFM phase up to the highest studied pressure of 170 GPa and S stripe up to 115 GPa by increasing pressure adiabatically [54]. Notably, the C-AFM state remains robust about 1.5 meV above the NM state while the magnetic moments weaken. At 170 GPa, $M_{\text{C-AFM}} = 0.13\mu_B$, but we expect the C-AFM phase to finally vanish at still higher pressures. The relative stability of the C-AFM configuration could be due to its ferromagnetic interlayer coupling [Fig. 1(c)], which allows covalent bonding between the magnetic Cu orbitals when the pressure moves the CuO_2 planes closer to each other.

Electronic structure under pressure. Figure 3(a) shows the $YBCO_7$ electronic structure at ambient pressure for the G-AFM state, which is typical of the cuprates—dominated by planar Cu $d_{x^2-y^2}$. Also, chain Cu d_{z^2} bands are present, but they only have negligible hybridization with the Cu_{pl} $d_{x^2-y^2}$ bands. The bilayer splitting leads to two distinct $d_{x^2-y^2}$ Fermi-surface rings that partly disappear due to unfolding into the primitive NM unit cell [55,56]. The d_{z^2} states display Hund's coupling with the $d_{x^2-y^2}$ bands [33], as seen from the spin polarization in the partial density of states (PDOS), and have a slight Fermi level contribution through hybridization with the $d_{x^2-y^2}$ and chain bands.

At 100 GPa, the d_{z^2} band rises to the Fermi level for both the metastable C-AFM state [Fig 3(b)] and the NM ground state [Fig. 3(c)]. This increases the Cu_{pl} d_{z^2} hole content at 100 GPa despite the decrease in the total Cu_{pl} hole content (see SM Sec. S3.3 [42] for details). The 100 GPa C-AFM state has little hybridization between the two d orbitals but

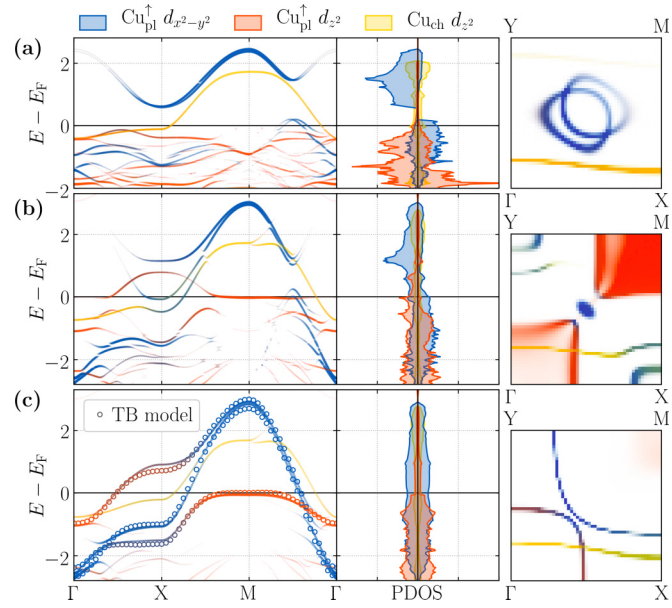

FIG. 3. Orbital-decomposed $YBCO_7$ electronic structures and Fermi surfaces (spectral functions at the Fermi energy) at $k_z = 0$ for Cu_{pl} $d_{x^2-y^2}$, Cu_{pl} d_{z^2}, and Cu_{ch} d_{z^2} for (a) $P = 0$ G-AFM phase ($M = 0.462\mu_B$), (b) 100 GPa C-AFM phase ($M = 0.326\mu_B$), and (c) 100 GPa NM phase. In the AFM cases the Cu_{pl} PDOS has been plotted only for ions with positive M and the energy bands and spectral functions have been unfolded into the primitive NM cell. The three highest bands of our four-band TB model are plotted for the 100 GPa NM case.

significant $d_{x^2-y^2}$–chain hybridization. The d_{z^2} bands are pinned to the Fermi level, possibly because they are pushed upwards by Hund's coupling but acquire holes at a slow rate. This flat band dominates the states at the Fermi energy ($k_z = 0$), but due to the slight three-dimensionality of the d_{z^2} bands this is less prominent for $k_z \neq 0$ (see SM Sec. S2.3 [42] for details). Once the magnetization is suppressed, in the NM phase, d_{z^2} and $d_{x^2-y^2}$ hybridize strongly around the X point (where the AFM bands overlap) and the $d_{x^2-y^2}$–chain hybridization is absent, contrary to the C-AFM case. The NM phase spectral function at Fermi energy has mainly $d_{x^2-y^2}$ and chain contributions and the d_{z^2} flat band is only weakly visible around M.

To explore the second dome physics under pressure, we have adopted a minimal NM tight-binding (TB) model that accounts for bilayer splitting and $d_{x^2-y^2}-d_{z^2}$ hybridization [57]. The model is overlaid in Fig. 3(c) for $P = 100$ GPa and plotted for $P = 0$ in SM Fig. S10 [42]. The model is based on using symmetric and antisymmetric intraorbital combinations, so that the Hamiltonian becomes block-diagonal. The strong bilayer splitting between the d_{z^2} orbitals shifts the antisymmetric d_{z^2} band to much lower energies. This separation keeps the antisymmetric d_{z^2} and $d_{x^2-y^2}$ bands from hybridizing. However, the symmetric bands remain close in energy, leading to the strong hybridization near the X point. Our symmetric bands are strikingly similar to Maier *et al.*'s model at $x = 0.85$ [8], which is within their second dome. The two TB models can be directly mapped onto each other with the exception of a few next-nearest-neighbor terms (see SM

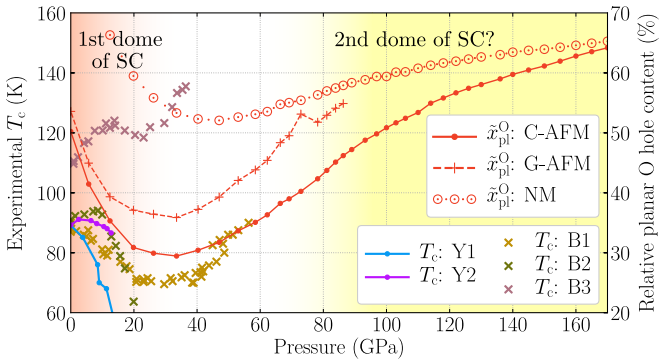

FIG. 4. Left axis: Experimental P dependence of T_c in selected samples. Y1: $YBCO_{6.98}$ [62]. Y2: $YBCO_{6+\delta}$ with δ estimated to be between 0.85 and 1.00 [63]. B1: Slightly overdoped $n = 2$ BSCCO [10]. B2 and B3: Optimally doped $n = 2$ [3] and $n = 3$ [28] BSCCO. Right axis: The fractional planar O hole content obtained from the Bader analysis as $\tilde{x}^{O}_{pl} = 2x(O_{pl})/x([CuO_2]_{pl})$.

Sec. S7 [42]). Based on this intimate connection, NM $YBCO_7$ at 100 GPa sits within the underdoped side of the second dome predicted by Ref. [8].

Importance of O_{pl} *hole content.* The long-sought explanation for the pairing mechanism in the first dome might have recently been verified to be superexchange [58], as proposed just a few months after the discovery of high-T_c's [59]. There is a correlation between the maximal T_c and the planar O hole content [60], which can be understood within the superexchange model [61]. In this spirit, we plot in Fig. 4 the fraction of the $YBCO_7$ oxygen holes within the CuO_2 planes ($\tilde{x}^{O}_{pl}$), as well as the available experimental T_c data, which we supplement with BSCCO data that extend to higher pressures. Below 20 GPa, the pressure-induced doping leads to the suppression of T_c in YBCO (Y1 and Y2) and $n = 2$ BSCCO samples (B1 and B2), which is consistent with these samples either being close to optimal doping or sitting on the overdoped side of the first SC dome. Pressure also causes $\tilde{x}^{O}_{pl}$ to decrease, which is consistent both with the superexchange model and Ref. [61], in that it shows a correlation between T_c and $\tilde{x}^{O}_{pl}$ for the first dome. However, recent $YBCO_{6.9}$ low-pressure Cu–O charge transfer results [64] based on nuclear magnetic resonance measurements [65] are somewhat different from our results (see SM Sec. S3.2 [42] for a discussion of this point).

Based on our TB analysis, we expect $YBCO_7$ to enter the second dome regime around 100 GPa. Even though experimental T_c data for $YBCO_7$ are limited, the B1 and B3 BSCCO data sets display a pressure-induced revival in SC above ~30 GPa. Also, $\tilde{x}^{O}_{pl}$ begins to increase with pressure, with striking similarity to the B1 data set. At 100 GPa, the $\tilde{x}^{O}_{pl}$ reaches the $P = 0$ AFM values, raising the possibility of a correlation between $\tilde{x}^{O}_{pl}$ and T_c in the second dome. If so, how does this affect the pairing mechanism? Here, there are many more possibilities than in the case of the first dome since both Cu $d_{x^2-y^2}$ and d_{z^2} are involved. Notably, Ref. [8] finds two pairing channels, d wave and $s^{\pm}$ wave, with both channels dominated by spin fluctuations of the d_{z^2} electrons. Scenarios for multiorbital pairing have been discussed in Ref. [6]. In the orbital fluctuation model—another early proposal for explaining high T_c—pairing between oxygen holes is mediated by the d orbitals [66–68], potentially explaining the importance of $\tilde{x}^{O}_{pl}$ and the oxygen holes for the second dome. Alternatively, the pressure-induced enhancement in $\tilde{x}^{O}_{pl}$ and intraplanar covalency could revive the superexchange mechanism for the second dome [61] or the d_{z^2} flat band could induce pairing-effective $s^{\pm}$ spin fluctuations [12], as discussed in SM Sec. S5.2 [42]. Finally, we note that the near degeneracy of the NM state with the metastable high-pressure C-AFM state could lead to enhanced pairing fluctuations.

Relationship with pseudogap collapse. Cuprates are characterized by a mysterious pseudogap phase that involves intertwined orders [69–73]. The abundance of near-degenerate stripe phases found in ambient-pressure $YBCO_7$ have been proposed to be a signature of the pseudogap phase [36]. Our results show that the multiplicity of these phases persists to high pressures, where these phases rise about 1.5 meV above the NM state (which is 54 meV above the ground state without pressure), indicating termination of the pseudogap phase. This is reminiscent of La_2CuO_4, where the NM phase is 150 meV above the ground state at zero doping [33] while the magnetic phases have been pushed up to 60 meV above the NM phase at 30% doping [74]. We also observe a Van Hove singularity crossing the Fermi level near 126 GPa, another signature of pseudogap collapse [75]. Note that the pseudogap collapse with pressure appears to be at a higher doping than that found in Ca-substituted YBCO [76], which may be due to pressure pushing the d_{z^2} band above the Fermi level while preserving the $d_{x^2-y^2}$ band occupation (see SM Sec. S5.1 [42] for discussion).

Using the prototypical stoichiometric cuprate superconductor $YBCO_7$, our study explores the in-depth evolution of the electronic structure on a first-principles basis when this cuprate is doped continuously via pressure to a higher Cu valency configuration with active d_{z^2} orbitals. Under high pressure (100 GPa), $YBCO_7$ is shown to become compatible with the second dome SC model proposed in Ref. [8]; the pressure could presumably be lowered below 100 GPa via chemical doping to allow access to the second dome under experimentally more accessible pressures. Our analysis show that pressure leads to significant intraplanar Cu–O hole transfer and indicates that the planar oxygen-hole content correlates with T_c for the second dome, as is the case for the first dome. All studied magnetic phases are found to become unstable around the pressure range of the proposed second dome in $YBCO_7$, which is a signature of pseudogap collapse, hinting at a new connection between the second dome and the pseudogap phase.

Acknowledgments. We thank Yubo Zhang for his contribution in the early phase of the work and Sugata Chowdhury for useful discussions. J.N. thanks Osk. Huttunen Foundation and INERCOM platform for financial support. The work at Northeastern University was supported by the U.S. Department of Energy (DOE), Office of Science, Basic Energy Sciences Grant No. DE-SC0022216 and benefited from Northeastern University's Advanced Scientific Computation Center and the Discovery Cluster and the National Energy Research Scientific Computing Center through U.S. DOE Grant No. DE-AC02-05CH11231. The work at Los Alamos National Laboratory was carried out under the auspices of

the U.S. DOE National Nuclear Security Administration under Contract No. 89233218CNA000001. It was supported by the LANL LDRD Program, the Quantum Science Center, a U.S. DOE Office of Science National Quantum Information Science Research Center, and in part by the Center for Integrated Nanotechnologies, a U.S. DOE BES user facility, in partnership with the LANL Institutional Computing Program for computational resources. Additional computations were performed at the National Energy Research Scientific Computing Center (NERSC), a U.S. DOE Office of Science User Facility located at Lawrence Berkeley National Laboratory, operated under Contract No. DE-AC02-05CH11231 using NERSC Award No. ERCAP0020494. The work at Tulane University was supported by the U.S. Office of Naval Research Grant No. N00014-22-1-2673. B.B. acknowledges support from the COST Action CA19108.

[1] Q. Q. Liu, H. Yang, X. M. Qin, Y. Yu, L. X. Yang, F. Y. Li, R. C. Yu, C. Q. Jin, and S. Uchida, Phys. Rev. B **74**, 100506(R) (2006).
[2] T. H. Geballe and M. Marezio, Phys. C: Superconductivity **469**, 680 (2009).
[3] X.-J. Chen, V. V. Struzhkin, Y. Yu, A. F. Goncharov, C.-T. Lin, H.-k. Mao, and R. J. Hemley, Nature (London) **466**, 950 (2010).
[4] Y. Zhong, Y. Wang, S. Han, Y.-F. Lv, W.-L. Wang, D. Zhang, H. Ding, Y.-M. Zhang, L. Wang, K. He, R. Zhong, J. A. Schneeloch, G.-D. Gu, C.-L. Song, X.-C. Ma, and Q.-K. Xue, Sci. Bull. **61**, 1239 (2016).
[5] K. Jiang, X. Wu, J. Hu, and Z. Wang, Phys. Rev. Lett. **121**, 227002 (2018).
[6] A. M. Oleś, K. Wohlfeld, and G. Khaliullin, Condens. Matter **4**, 46 (2019).
[7] W. M. Li, J. F. Zhao, L. P. Cao, Z. Hu, Q. Z. Huang, X. C. Wang, Y. Liu, G. Q. Zhao, J. Zhang, Q. Q. Liu, R. Z. Yu, Y. W. Long, H. Wu, H. J. Lin, C. T. Chen, Z. Li, Z. Z. Gong, Z. Guguchia, J. S. Kim, G. R. Stewart *et al.*, Proc. Natl. Acad. Sci. USA **116**, 12156 (2019).
[8] T. Maier, T. Berlijn, and D. J. Scalapino, Phys. Rev. B **99**, 224515 (2019).
[9] D. J. Scalapino, Proc. Natl. Acad. Sci. USA **116**, 12129 (2019).
[10] L. Deng, Y. Zheng, Z. Wu, S. Huyan, H.-C. Wu, Y. Nie, K. Cho, and C.-W. Chu, Proc. Natl. Acad. Sci. USA **116**, 2004 (2019).
[11] S. D. Conradson, T. H. Geballe, C. Jin, L. Cao, G. Baldinozzi, J. M. Jiang, M. J. Latimer, and O. Mueller, Proc. Natl. Acad. Sci. USA **117**, 4565 (2020).
[12] K. Matsumoto, D. Ogura, and K. Kuroki, J. Phys. Soc. Jpn. **89**, 044709 (2020).
[13] L. Sederholm, S. D. Conradson, T. H. Geballe, C.-Q. Jin, A. Gauzzi, E. Gilioli, M. Karppinen, and G. Baldinozzi, Condens. Matter **6**, 50 (2021).
[14] M. Zegrodnik, P. Wójcik, and J. Spałek, Phys. Rev. B **103**, 144511 (2021).
[15] W. E. Pickett, Rev. Mod. Phys. **61**, 433 (1989).
[16] T. Das and C. Panagopoulos, New J. Phys. **18**, 103033 (2016).
[17] M. Shimizu, N. Takemori, D. Guterding, and H. O. Jeschke, Phys. Rev. Lett. **121**, 137001 (2018).
[18] P. Reiss, D. Graf, A. A. Haghighirad, W. Knafo, L. Drigo, M. Bristow, A. J. Schofield, and A. I. Coldea, Nat. Phys. **16**, 89 (2020).
[19] F. Du, S. Luo, B. R. Ortiz, Y. Chen, W. Duan, D. Zhang, X. Lu, S. D. Wilson, Y. Song, and H. Yuan, Phys. Rev. B **103**, L220504 (2021).
[20] K. Y. Chen, N. N. Wang, Q. W. Yin, Y. H. Gu, K. Jiang, Z. J. Tu, C. S. Gong, Y. Uwatoko, J. P. Sun, H. C. Lei, J. P. Hu, and J.-G. Cheng, Phys. Rev. Lett. **126**, 247001 (2021).
[21] J. Liu, Q.-W. Wang, and L.-J. Zou, Phys. Lett. A **391**, 127118 (2021).
[22] A. C. Mark, J. C. Campuzano, and R. J. Hemley, High Press. Res. **42**, 137 (2022).
[23] J. S. Schilling, *Handbook of High-Temperature Superconductivity: Theory and Experiment* (Springer, Berlin, 2007), pp. 427–462.
[24] N. Poccia, G. Campi, M. Fratini, A. Ricci, N. L. Saini, and A. Bianconi, Phys. Rev. B **84**, 100504(R) (2011).
[25] I. Zeljkovic, J. Nieminen, D. Huang, T.-R. Chang, Y. He, H.-T. Jeng, Z. Xu, J. Wen, G. Gu, H. Lin, R. S. Markiewicz, A. Bansil, and J. E. Hoffman, Nano Lett. **14**, 6749 (2014).
[26] D. Song, X. Zhang, C. Lian, H. Liu, I. Alexandrou, I. Lazić, E. G. T. Bosch, D. Zhang, L. Wang, R. Yu, Z. Cheng, C. Song, X. Ma, W. Duan, Q. Xue, and J. Zhu, Adv. Funct. Mater. **29**, 1903843 (2019).
[27] R. Matsumoto, S. Yamamoto, Y. Takano, and H. Tanaka, ACS Omega **6**, 12179 (2021).
[28] Y. Zhou, J. Guo, S. Cai, J. Zhao, G. Gu, C. Lin, H. Yan, C. Huang, C. Yang, S. Long, Y. Gong, Y. Li, X. Li, Q. Wu, J. Hu, X. Zhou, T. Xiang, and L. Sun, Nat. Phys. **18**, 406 (2022).
[29] P. E. Blöchl, Phys. Rev. B **50**, 17953 (1994).
[30] G. Kresse and D. Joubert, Phys. Rev. B **59**, 1758 (1999).
[31] G. Kresse and J. Furthmüller, Phys. Rev. B **54**, 11169 (1996).
[32] J. Sun, A. Ruzsinszky, and J. P. Perdew, Phys. Rev. Lett. **115**, 036402 (2015).
[33] C. Lane, J. W. Furness, I. G. Buda, Y. Zhang, R. S. Markiewicz, B. Barbiellini, J. Sun, and A. Bansil, Phys. Rev. B **98**, 125140 (2018).
[34] J. W. Furness, Y. Zhang, C. Lane, I. G. Buda, B. Barbiellini, R. S. Markiewicz, A. Bansil, and J. Sun, Commun. Phys. **1**, 11 (2018).
[35] J. Nokelainen, C. Lane, R. S. Markiewicz, B. Barbiellini, A. Pulkkinen, B. Singh, J. Sun, K. Pussi, and A. Bansil, Phys. Rev. B **101**, 214523 (2020).
[36] Y. Zhang, C. Lane, J. W. Furness, B. Barbiellini, J. P. Perdew, R. S. Markiewicz, A. Bansil, and J. Sun, Proc. Natl. Acad. Sci. USA **117**, 68 (2020).
[37] A. N. Tatan, J. Haruyama, and O. Sugino, AIP Adv. **12**, 105308 (2022).
[38] K. Pokharel, C. Lane, J. W. Furness, R. Zhang, J. Ning, B. Barbiellini, R. S. Markiewicz, Y. Zhang, A. Bansil, and J. Sun, npj Comput. Mater. **8**, 31 (2022).
[39] R. Zhang, C. Lane, J. Nokelainen, B. Singh, B. Barbiellini, R. S. Markiewicz, A. Bansil, and J. Sun, arXiv:2207.00184 [Phys. Rev. Lett. (to be published)].
[40] Z. Jin and S. Ismail-Beigi, arXiv:2309.07997 (2023).

[41] J. Ning, C. Lane, B. Barbiellini, R. S. Markiewicz, A. Bansil, A. Ruzsinszky, J. P. Perdew, and J. Sun, J. Chem. Phys. **160**, 064106 (2024).

[42] See Supplemental Material at http://link.aps.org/supplemental/10.1103/PhysRevB.110.L020502 for additional figures, data analysis, and extended discussions to support the findings presented in the main manuscript, which includes Refs. [77–81].

[43] M. Calamiotou, A. Gantis, D. Lampakis, E. Siranidi, E. Liarokapis, I. Margiolaki, and K. Conder, Europhys. Lett. **85**, 26004 (2009).

[44] M. Calamiotou, A. Gantis, E. Siranidi, D. Lampakis, J. Karpinski, and E. Liarokapis, Phys. Rev. B **80**, 214517 (2009).

[45] H. Sakakibara, K. Suzuki, H. Usui, K. Kuroki, R. Arita, D. J. Scalapino, and H. Aoki, Phys. Rev. B **86**, 134520 (2012).

[46] W. Tang, E. Sanville, and G. Henkelman, J. Phys.: Condens. Matter **21**, 084204 (2009).

[47] M. Yu and D. R. Trinkle, J. Chem. Phys. **134**, 064111 (2011).

[48] The value $x([CuO_2]_{pl}) = 0.11$ holes is smaller than the value 0.18 holes found in the literature for $YBCO_7$ [79]; this difference is discussed in SM Sec. S3.1 [42].

[49] J. Jorgensen, S. Pei, P. Lightfoot, D. Hinks, B. Veal, B. Dabrowski, A. Paulikas, R. Kleb, and I. Brown, Phys. C: Superconductivity **171**, 93 (1990).

[50] C. C. Almasan, S. H. Han, B. W. Lee, L. M. Paulius, M. B. Maple, B. W. Veal, J. W. Downey, A. P. Paulikas, Z. Fisk, and J. E. Schirber, Phys. Rev. Lett. **69**, 680 (1992).

[51] S. Sadewasser, J. S. Schilling, A. P. Paulikas, and B. W. Veal, Phys. Rev. B **61**, 741 (2000).

[52] O. Cyr-Choinière, D. LeBoeuf, S. Badoux, S. Dufour-Beauséjour, D. A. Bonn, W. N. Hardy, R. Liang, D. Graf, N. Doiron-Leyraud, and L. Taillefer, Phys. Rev. B **98**, 064513 (2018).

[53] This stripe phase was the most stable 2×3 or 3×2 stripe phase in our pressure tests (see SM Sec. S4 [42] for details). Larger stripe phases could be energetically more favorable at zero pressure [36] or the paramagnetic phase could be energetically more favorable over the NM phase at high pressures but considering these phases was not feasible due to computational reasons.

[54] At these pressures these states become fragile and can be preserved only with the most accurate technical settings (see SM Sec. S1.4 [42] for details).

[55] W. Ku, T. Berlijn, and C.-C. Lee, Phys. Rev. Lett. **104**, 216401 (2010).

[56] U. Herath, P. Tavadze, X. He, E. Bousquet, S. Singh, F. Muñoz, and A. H. Romero, Comput. Phys. Commun. **251**, 107080 (2020).

[57] M. Baublitz, C. Lane, H. Lin, H. Hafiz, R. S. Markiewicz, B. Barbiellini, Z. Sun, D. S. Dessau, and A. Bansil, Sci. Rep. **4**, 7512 (2014).

[58] S. M. O'Mahony, W. Ren, W. Chen, Y. X. Chong, X. Liu, H. Eisaki, S. Uchida, M. H. Hamidian, and J. C. S. Davis, Proc. Natl. Acad. Sci. USA **119**, e2207449119 (2022).

[59] P. W. Anderson, Science **235**, 1196 (1987).

[60] D. Rybicki, M. Jurkutat, S. Reichardt, C. Kapusta, and J. Haase, Nat. Commun. **7**, 11413 (2016).

[61] N. Kowalski, S. S. Dash, P. Sémon, D. Sénéchal, and A.-M. Tremblay, Proc. Natl. Acad. Sci. USA **118**, e2106476118 (2021).

[62] P. L. Alireza, G. H. Zhang, W. Guo, J. Porras, T. Loew, Y.-T. Hsu, G. G. Lonzarich, M. Le Tacon, B. Keimer, and S. E. Sebastian, Phys. Rev. B **95**, 100505(R) (2017).

[63] S. Klotz, W. Reith, and J. Schilling, Phys. C: Superconductivity **172**, 423 (1991).

[64] M. Jurkutat, C. Kattinger, S. Tsankov, R. Reznicek, A. Erb, and J. Haase, Proc. Natl. Acad. Sci. USA **120**, e2215458120 (2023).

[65] J. Haase, O. P. Sushkov, P. Horsch, and G. V. M. Williams, Phys. Rev. B **69**, 094504 (2004).

[66] W. Weber, Z. Phys. B **70**, 323 (1988).

[67] M. Jarrell, H. R. Krishnamurthy, and D. L. Cox, Phys. Rev. B **38**, 4584 (1988).

[68] D. L. Cox, M. Jarrell, C. Jayaprakash, H. R. Krishna-murthy, and J. Deisz, Phys. Rev. Lett. **62**, 2188 (1989).

[69] E. Fradkin, S. A. Kivelson, and J. M. Tranquada, Rev. Mod. Phys. **87**, 457 (2015).

[70] R. M. Fernandes, P. P. Orth, and J. Schmalian, Annu. Rev. Condens. Matter Phys. **10**, 133 (2019).

[71] B. Michon, C. Girod, S. Badoux, J. Kačmarčík, Q. Ma, M. Dragomir, H. A. Dabkowska, B. D. Gaulin, J.-S. Zhou, S. Pyon, T. Takayama, H. Takagi, S. Verret, N. Doiron-Leyraud, C. Marcenat, L. Taillefer, and T. Klein, Nature (London) **567**, 218 (2019).

[72] M. Lizaire, A. Legros, A. Gourgout, S. Benhabib, S. Badoux, F. Laliberté, M.-E. Boulanger, A. Ataei, G. Grissonnanche, D. LeBoeuf, S. Licciardello, S. Wiedmann, S. Ono, H. Raffy, S. Kawasaki, G.-Q. Zheng, N. Doiron-Leyraud, C. Proust, and L. Taillefer, Phys. Rev. B **104**, 014515 (2021).

[73] R. S. Markiewicz and A. Bansil, Phys. Rev. B **109**, 045116 (2024).

[74] S. Wakimoto, K. Yamada, J. M. Tranquada, C. D. Frost, R. J. Birgeneau, and H. Zhang, Phys. Rev. Lett. **98**, 247003 (2007).

[75] R. S. Markiewicz and A. Bansil, arXiv:2303.11254 (2023).

[76] J. Loram, J. Luo, J. Cooper, W. Liang, and J. Tallon, J. Phys. Chem. Solids **62**, 59 (2001).

[77] J. P. Perdew, K. Burke, and M. Ernzerhof, Phys. Rev. Lett. **77**, 3865 (1996).

[78] R. Poloni, A. L. Mariano, D. Prendergast, and J. Garcia-Barriocanal, J. Chem. Phys. **149**, 234706 (2018).

[79] R. Liang, D. A. Bonn, and W. N. Hardy, Phys. Rev. B **73**, 180505(R) (2006).

[80] N. P. Ong, Z. Z. Wang, J. Clayhold, J. M. Tarascon, L. H. Greene, and W. R. McKinnon, Phys. Rev. B **35**, 8807 (1987).

[81] I. Zeljkovic, Z. Xu, J. Wen, G. Gu, R. S. Markiewicz, and J. E. Hoffman, Science **337**, 320 (2012).